



# Framework for Capturing and Editing of Anisotropic Effect Coatings

J. Filip,<sup>1</sup> R. Vávra,<sup>1</sup> F. J. Maile<sup>2</sup> and M. Kolafová<sup>1</sup>

<sup>1</sup>The Czech Academy of Sciences, Institute of Information Theory and Automation, Czech Republic  
{filipj, vavra, kolafova}@utia.cas.cz

<sup>2</sup>Schlenk Metallic Pigments, GmbH, Germany  
frankjochen.maile@schlenk.de

---

## Abstract

Coatings are used today for products, ranging from automotive production to electronics and everyday use items. Product design is taking on an increasingly important role, where effect pigments come to the fore, offering a coated surface extra optical characteristics. Individual effect pigments have strong anisotropic, azimuthally-dependent behaviour, typically suppressed by a coating application process, randomly orienting pigment particles resulting in isotropic appearance. One exception is a pigment that allows control of the azimuthal orientation of flakes using a magnetic field. We investigate visual texture effects due to such an orientation in a framework allowing efficient capturing, modelling and editing of its appearance. We captured spatially-varying BRDFs of four coatings containing magnetic effect pigments. As per-pixel non-linear fitting cannot preserve coating sparkle effects, we suggest a novel method of anisotropy modelling based on images shifting in an angular domain. The model can be utilized for a fast transfer of desired anisotropy to any isotropic effect coating, while preserving important spatially-varying visual features of the original coating. The anisotropic behaviour was fitted by a parametric model allowing for editing of coating appearance. This framework allows exploration of anisotropic effect coatings and their appearance transfer to standard effect coatings in a virtual environment.

**Keywords:** appearance modelling, modelling, reflectance and shading models, rendering, texture synthesis, rendering

**CCS Concepts:** • Computing methodologies → Reflectance modelling; Texturing

---

## 1. Introduction

A wide range of industries like automotive, consumer electronics, textile or architecture have started to use of effect pigments in coatings, plastics and printing inks over the last decades with the intention to increase the attractiveness of product appearance. Effect pigments are also often used in printing inks or 3D printing filaments that allow artists or computer graphics professionals and researchers to create eye-catching posters and objects. Effect pigments can be considered as tiny particles of anisotropic morphology in the size range of 1–200 microns (diameter D50). Their shape, material or orientation in media, relative to coating applications, determine a coatings final visual appearance [MPR05, Pfa08]. Effect pigments are frequently used to underline and enhance a 3D-object's shape (i.e. concave/convex structures), as they visually boost three-dimensional object shape due to their interaction with light, which leads to angle-dependent optical properties originating in their particle design and anisotropic morphology. Colour designers use these pigments, in combination with other components, to create the de-

sired colour and texture effect. Resulting fine-scale texture is due to individual particles acting as highly reflective mirrors, producing directionally dependent anisotropic texture effect. This effect originating from the effect pigment particles (e.g. in the polymer layer of the effect coating) is often denoted in industry as *sparkle* (see Figure 2). This sparkle effect is still visible in a distance of several meters from the object; therefore, the visually correct representation of spatially-varying information is essential for effect coatings appearance reproduction.

Although, in recent decades, the coating industry has made a great progress in improving coating appearances, current coating technology could serve to create even more attractive colours and appearances of products. However, industry cannot embrace them yet due to a lack of reliable quality control methods to control complicated effect coatings. While current industrial coating application procedures can control and predict the particle orientation within the coating layer relatively well, they cannot easily orient them on a large scale in a particular azimuthal direction. Therefore,

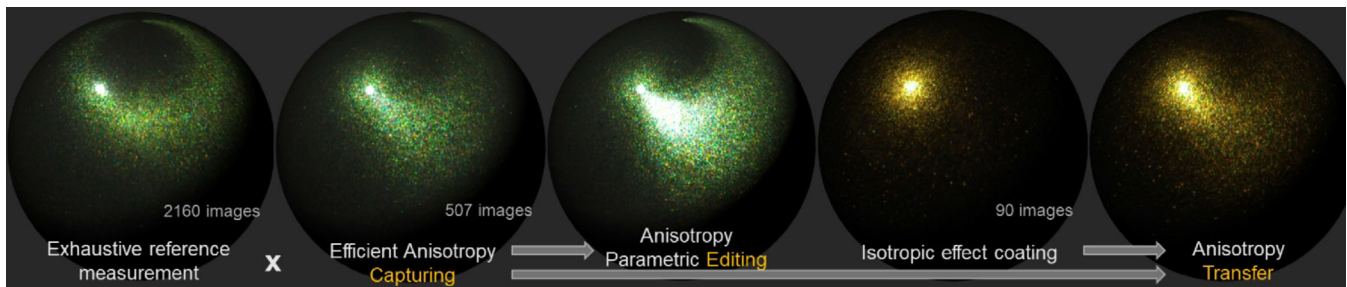


**Figure 1:** The proposed framework for capture, edit, and transfer of anisotropic behaviour in effect coatings.

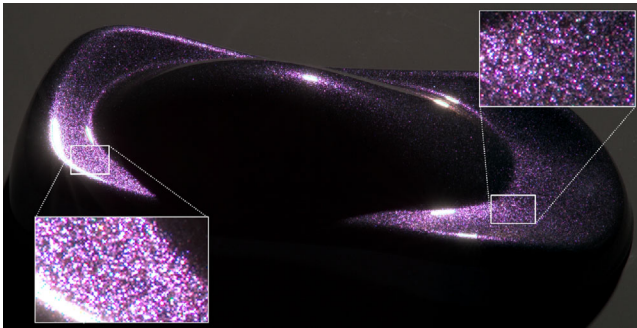


**Figure 2:** An example of effect coating on a dummy car shape.

a majority of coatings based on effect pigments, have a close-to-random azimuthal distribution of particle orientations in a basecoat, causing an isotropic, i.e. azimuthally-independent appearance.

In contrast to the majority of particles in the family of effect pigments, particles with magnetic properties (either magnetizable or intrinsically magnetic) allow to influence their azimuthal orientation applying an electromagnetic field [PLMR17]. If the mentioned influence allows to control effect pigment particle orientation, it is possible to achieve and explore so far unknown surface appearance properties. A known problem in industry is the effort undertaken to modify and improve a coating formulation and to create physical samples which slows down development times. Economically and environmentally it would be an improvement to digitize this visualization process. This is the reason why image-based measurements of small, planar specimens are used for the digital capturing and appearance editing of the real-world effect coatings.

In this paper, we analyse effects pigments that can be oriented in a magnetic field. This controlled pigment orientation creates anisotropic behaviour of the coating manifested by variable appearance with respect to sample rotation for fixed illumination and observation geometry. We capture this behaviour by employing spatially-varying BRDFs. As per-pixel non-linear BRDF fitting did not preserve sparkle effect, we propose a parametric model that can transfer this material- or user-defined- anisotropic appearance to almost any type of standard effect coating as shown in Fig. 1. This model demonstrates how effect coatings with random azimuthal particle orientation would look, once one is able to align their effect particles to a specific azimuthal direction, and thus allows designers to

assess overall appearance of the product in a virtual environment by merely using a combination of previously captured planar samples.

Our analysis utilizes a half-difference angular parameterization [Rus98] that can be applied to effect coatings with a nearly-flat random structure, captured as a spatially-varying BRDF. The main contributions of this paper are:

- method of capturing pigment coatings with magnetic properties using only two slices of spatially-varying BRDF,
- a parametric method of captured coatings' anisotropic behaviour representation and editing,
- an application of anisotropic behaviour transfer introducing such appearance to ordinary effect coatings. This demonstrates the coating appearances that could be achieved by a directional alignment of their pigment particles.

## 2. Related Work

Our work is related to the colour design, physical models of anisotropic appearance, its perception and fabrication and finally to appearance capturing of effect coatings.

Colour and trim designers in many cases only use specific visually important features such as face or flop, as they are the most prominent features in colour communication. The *face* represents the reflective nature of coatings under near to normal viewing directions, when light path length is minimized and thus lacking a colour contribution typical for *flop*, i.e. far from normal viewing angles, where light travels a longer path in the coating layer and substantially interacts with surfaces of the flakes. Shimizu *et al.* [SM10] proposed an intuitive tool for the rapid colour design of automotive colours by picking face and flop colours from so called virtual mood boards. Authors [SM15] further suggest a computer aided system for designing colour appearance of metallic automotive coatings. The final design is specified in terms of industrial measurement standards for metallic colour appearance, and paint formulations are determined by employing an automotive refinish system.

However, anisotropic appearance introduces additional dimensions as material appearance changes with respect to surface rotation around its normal. Although such materials can be effectively captured using SVBRDFs, e.g. [DWT\*10, CDP\*14], their realistic modelling is much more challenging than for isotropic ones. With respect to development of more accurate material anisotropic models, theories of micro-facets and micro-flake physics applicable to

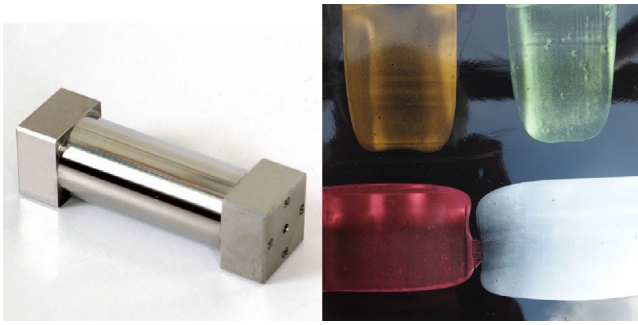


**Figure 3:** Cylindrical film applicator (left) and four different pigments applied on a plastic material with black glossy basecoat (right).

BRDF [NRH\*77] and spatially-varying BRDF modelling [DHD16] were studied. This effort has been even extended to the reproduction of spatially-varying effects of microstructure anisotropic effects like scratches and glints. Yan *et al.* [YHJ\*14] presented method for glint modelling using per-pixel normal distribution function based Gaussian pixel filter. Follow-up research applied to this task position-normal distributions [YHMR16] and wave optics model [YHW\*18]. Werner *et al.* [WVJH17] and Velinov *et al.* [VWH18] proposed a wave-optical shading models to render microscopic scratches including iridescent colours resulting from light diffraction. Although these methods produce realistic and visually plausible appearance, they do not attempt to fit real measured data. Alternative avenues of anisotropic micro-geometry modelling are generative learning models such as [KHx\*19] or mixtures of spherical Gaussians [XSD\*13]. Layered models are also becoming popular in representing certain classes of coatings [JdJM14] [ZJ18], [Bel18]; however, they are still limited to homogeneous appearance without surface texture, which is not the case of effect coatings.

Past research studied psychophysical aspects of visual anisotropy [HHE08, OVW11] and created statistical models describing the relationship between perceived and computational textural anisotropy [Koe84, WH04, OVW11] or directionality [SPGC08]. The prediction of anisotropic highlights locations has already been studied [LKK00] and recently further extended to arbitrary geometry with interactive tangents editing [RGB\*14]. Filip and Vávra focused on anisotropic highlight detection for the purpose of anisotropic materials adaptive measurement [FV15], and on analysis as to what extent people can detect anisotropy in rendered images [Fil15]. Filip and Kolafova [FK18] have shown that car body observers systematically prefer a certain orientation of anisotropy axis regardless of the surrounding illumination.

When it comes to fabrication of spatially-varying anisotropic reflectance functions different approaches exist. Weyrich *et al.* [WPMR09] suggested creating a customized reflectance function by changing the statistics of surface facets using a high-resolution metal milling process. Malzbender *et al.* [MSS\*12] used a combination of specular dimples and transparency film, and Lans *et al.* [LDPT13] proposed creation of a custom anisotropic spatially-varying appearance by means of a 3D printer to fabricate the facets and a flatbed UV printer to coat them with inks. Pereira *et al.*

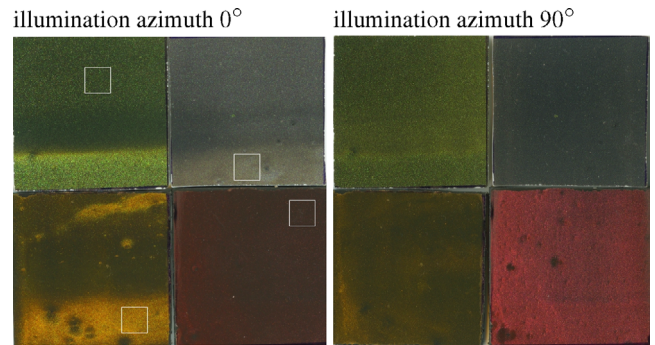


**Figure 4:** Appearance of the four applied pigments when observed from top view and fixed light at elevation 45° for two different illumination azimuthal angles. See distinct horizontal boundaries in the samples which are due to swiping a magnet under the sample. White frames locate tiles used for analysis and visualization.

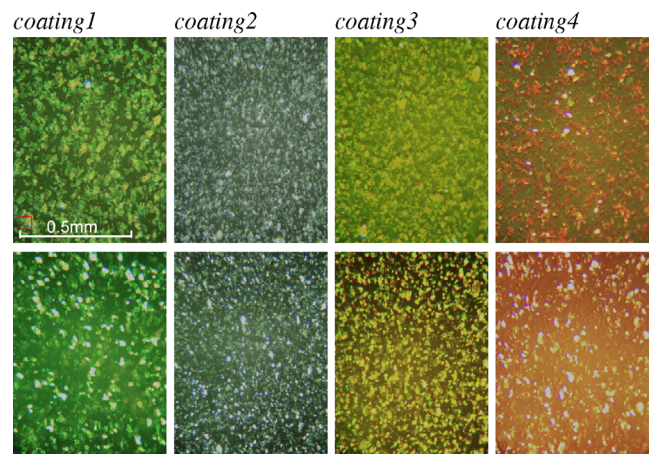


**Figure 5:** Microscopic images of pigment flakes for two azimuthal illumination 90 degrees apart. The red square in top-left image shows size of a single captured pixel.

[PLMR17] suggested fabrication of custom anisotropic BRDFs by using magnetic pigments in a time-varying magnetic field and photo-cured resin.

Finally, capturing of effect coatings is very challenging, due to different physical principles used to drive resulting visual appearance. Effect pigments can be, based on the principle of chroma and sparkling effect generation, roughly divided into three categories [MPR05, Pfa08]: metallic, interference and diffractive pigments. Metallic pigments rely mainly on geometrical properties of flakes and their reflectance, interference pigments introduce effects due to light wave interference with transparent substrate coated with materials of high refractive indices, and diffraction pigments decompose light at a diffraction grating of a frequency close to the wavelength of the incoming light. Note that in practice many effect coatings are often combinations of the above classes. Lans *et al.* [LKH12] presented an empirical approach to the realistic modelling of special effect flakes fitting patch-based model parameters using sparse texture data obtained by a portable multi-angle spectrophotometer. Rump

et al. [RSK09] presented extensions towards gonioapparent coatings texture measurement and modelling using bidirectional texture function (BTF) [DvGNK99]. Our work is closely related to work of Filip and Vávra [FV19] comparing several approaches to SVBRDF capturing of effect coatings using half-difference parameterization.

We are not aware of any work allowing capture, edit and transfer of anisotropic appearance of textured effect coatings.

### 3. Test Dataset Creation

To create a test set of coatings with anisotropic properties, we used four different pigments with magnetic properties in powder and unified their orientation by application of a magnetic field. A composition of the powder and resin was applied using a cylindrical film applicator (see Figure 3-left). As a base material, we used a 2-mm-thick plastic sheet with black glossy basecoat. A layer of approximately 100  $\mu\text{m}$  thickness was created by the uniform movement of the applicator over a small portion of liquid coating material applied on a plastic sheet. Although pigment manufacturers suggest using UV-curable resin, when under-curing occurred, we resorted to a standard waterborne resin. For this the drying process took about 10 s, which was sufficient time to unify the orientation of pigment particles by swiping a magnet under half of the painted area. For our experiments we used a 4x1 cm neodymium magnet in direct contact with the flip side of the painted plastic sheet which was moved in the direction of the paint application. The applied and dried coating layers can be seen in Figure 3-right which clearly shows application flow lines which result from the movement of the magnet.

From these samples based on differently coated sheets shown in Figure 3-right, we cut four samples of size 50  $\times$  50 mm, and initially analysed their anisotropic behaviour in a flatbed which captured appearance from a frontal viewing direction for an illumination elevation of approximately 45°. Figure 4 shows appearance behaviour for two different orientations of samples, i.e. different illumination azimuths. In the image there are apparent boundaries due to the magnet being swiped under the coating. More detailed information of appearance change due to lighting azimuth (rows) on pigment level is shown in microscopy images in Figure 5. An interesting finding was that particles are partially oriented, i.e. not randomly scattered, already after the application, without using the magnet. This is probably due to the fact that pigments are magnetic, and they are already uniformly oriented by swiping the metal applicator above the liquid coating.

### 4. Measurement of Anisotropic Effect Coatings

In the next step, we captured the spatially-varying appearance of these four samples using the half-difference parameterization [Rus98]. Due to typically low appearance variation along  $\varphi_d$  in BRDF and coatings as suggested in [FV19], we fixed the azimuthal angle of illumination direction relative to half-direction. We fixed  $\varphi_d = 90^\circ$  to obtain the majority of the effective hemisphere around a half-direction above plane defined by the measured sample normal as reported by [Bur]. As a result, we sampled only three angles  $\theta_h \times \theta_d \times \varphi_h$  as shown as three-dimensions in Figure 6.

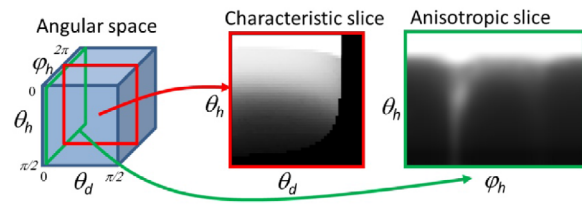


**Figure 6:** Angular slices in half-difference parameterization for fixed  $\varphi_d = 0^\circ$ .

Sampling of all three angles uniformly in step 5° would result to  $18 \times 18 \times 72 = 23,328$  images, which is inconvenient in practical scenarios. To create a sensible reference data, we considered typically smaller variations along  $\theta_d$  and  $\varphi_h$  and, based on psychophysical thresholds suggested in [FV19], reduced the sampling steps to  $[\Delta\theta_h, \Delta\theta_d, \Delta\varphi_h] = [5^\circ, 15^\circ, 15^\circ]$ . This configuration resulted in  $n_{\theta_h} \times n_{\theta_d} \times n_{\varphi_h} = 18 \times 5 \times 24 = 2160$  images.

For each pair of sampled incoming and outgoing directions, we captured an HDR image of the measured material of resolution 42  $\mu\text{m}/\text{pixel}$ . We used a four-axis gonioreflectometer [FVH\*13] consisting of two independent arms (with LED light and camera) and a turntable with the measured sample. The size of the sample was 40  $\times$  40 mm, distance to the camera was 2 m, and distance to the light, 1.5 m. The device was geometrically and colorimetrically calibrated, and the measured flat sample normal was accurately aligned within the coordinate system of the device. Repeatability of camera and light positioning is 0.03°. Capturing process of 2160 reference images took 6.5 h.

Due to our experimental coating application method, the appearance of the coating was not uniform across the entire sample (see Figure 4). Therefore, we manually selected a uniform area of 150  $\times$  150 pixels (corresponding to 6.3  $\times$  6.3 mm) in the captured images that was cut out (see white frames in Figure 4-left). As some of the selected areas still lack spatial uniformity in hue and luminance, we carefully removed their lowest frequency components in Fourier space. This step, to a certain extent, avoids a visually distractive tile repetition due to the non-uniformity of the coating application.

### 5. Per-Pixel Non-Linear Fitting

For the first straightforward attempt, we applied a per-pixel fitting of analytical anisotropic BRDF models. Various anisotropic models were tested: Ashikhmin–Shirley, Ashikhmin–Premoze, Kurt, Lafortune, Ward [GGG\*16]. To obtain stable fitting, an input per-pixel data were normalized and intensity values remapped using a median pixel BRDF as suggested in [NJR15]. We performed a number of experiments iteratively fitting 2-5 monospectral reflectance lobes and RGB diffuse and specular parameters using `mincon()` procedure and SQP algorithm in MATLAB. Our results have shown problems with the fitting stability and once stable results were achieved, did not model original pixel behaviour with sufficient quality. The main reason is the scattered reflectance distribution in individual pixels as shown in top part of Figure 8, which could be due to: (1) low optical resolution that caused the presence of several flakes with different orientations in each pixel (see approximate size of one pixel shown

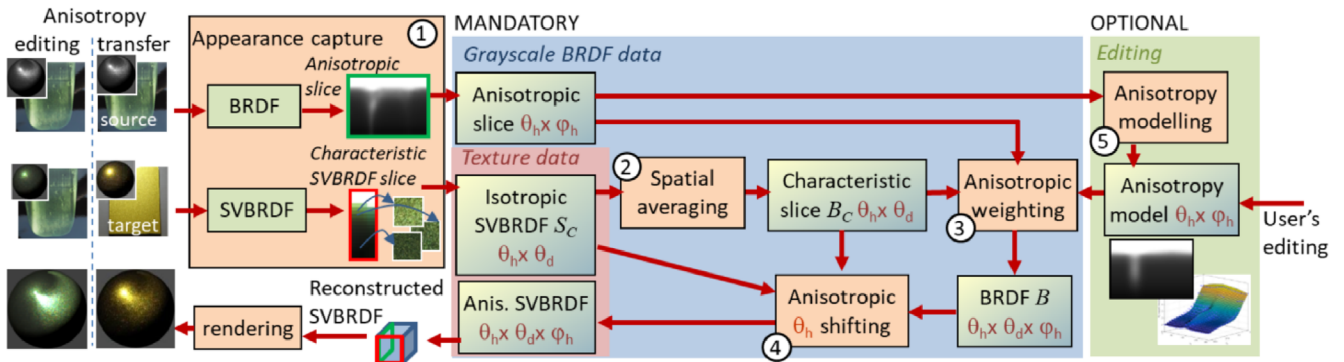


Figure 7: Overall scheme of our anisotropy modelling approach of spatially-varying effect coatings.

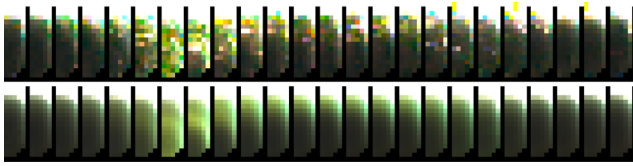


Figure 8: Top image—Captured BRDF data of single pixel. Bottom image—Pixel data fitting using Ashikhmin–Shirley model.

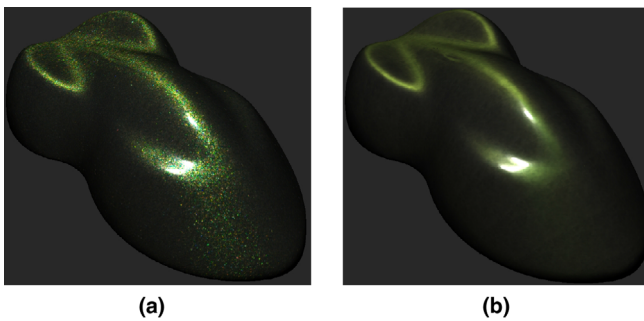


Figure 9: A comparison of renderings of (a) captured and (b) per-pixel fitted SV-BRDF of coating4.

as red square in Figure 5), (2) measurement inaccuracies due to a slight misalignment of images during the registration process, (3) colour artefacts due to exciting only a single pixel in Bayer pattern of our RGB sensor. Obtained fitting shown in bottom part of Figure 8 filters out possible errors, however, also the desired sparkle behaviour producing flat rendering as shown in Figure 9. Therefore, we resorted to an approach not relying on per-pixel intensity continuity in angular domain.

## 6. The Proposed Framework

An overview of the proposed anisotropic model is given in Figure 7. It starts with measurement of anisotropic and characteristic slices of the input material. While the anisotropic BRDF slice is captured only in gray scale values, the characteristic SVBRDF slice comprises a collection of colour texture images. First, we com-

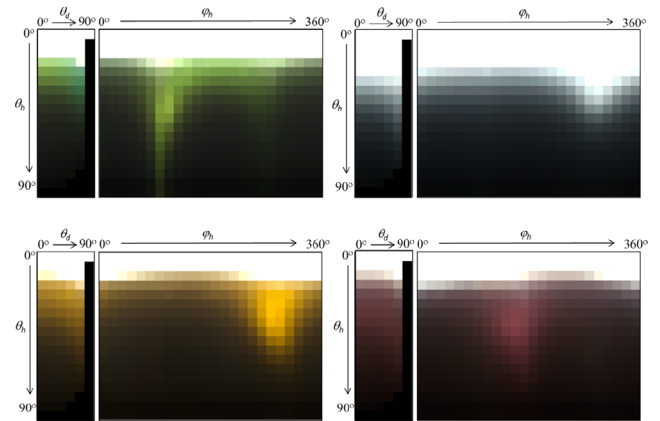
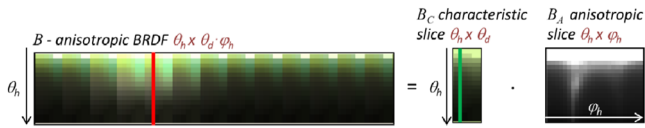


Figure 10: Four captured magnetic pigments: BRDF values of characteristic (left) and anisotropic (right) slices for  $\theta_d = 0^\circ$ , respectively.

pute a monospectral BRDF version of a characteristic slice which is combined with the anisotropic slice to efficiently approximate a monospectral BRDF of the material. Then, we use this BRDF and SVBRDF of a characteristic slice for the reproduction of an original material's anisotropic behaviour. The sections' numbering follows the ones on blocks in Figure 7.

① **Efficient anisotropic appearance measurement** – To make the measurement process even faster while still preserving main visual attributes of coatings, we captured only two angular slices. The first one, is an *anisotropic slice*, describing retro-reflective responses of material for variable azimuths similar to the parameterization of Dupuy nad Wenzel [DJ18]. We sampled  $\theta_h \times \varphi_h$  for fixed  $\theta_d = 0^\circ$ , describing azimuthally dependent behaviour of the sample (see the green part of Figure 6). The second one, is a *characteristic slice*  $\theta_h \times \theta_d$  [MHH\*12], capturing bivariate isotropic behaviour of material [RVZ08], especially the shape of a specular highlight (see the red part of Figure 6). To capture a typical azimuthal behaviour we needed to fix angle  $\varphi_h$ , for which we record the characteristic slice. To this end, we compute mean intensity of all columns of the anisotropic slice and select  $\varphi_h$  corresponding to the column having the most similar intensity to the mean one.



**Figure 11:** A composition of BRDF from characteristic and anisotropic slices.

The proposed angular configuration results in  $18 \times 24 = 432$  images for capturing the anisotropic slice, and  $18 \times 5 = 90$  images for capturing the characteristic slice. Due to redundancy in the slices, only 507 images are needed. Capturing the data needed only in characteristic and anisotropic slices took 1.5 h. In fact, the anisotropic slice can be recorded only as a gray scale BRDF, so one needs 417 BRDF values and 90 HDR images. This may further speed-up capturing by devices allowing faster sampling of BRDF values instead of images.

Figure 10 shows BRDF values of captured characteristic (left) and anisotropic (right) slices, obtained by spatial averaging of individual images. In anisotropic slices that are clearly visible, there are significant material-specific variations of hue and intensity across different azimuthal angles  $\varphi_h$ . They demonstrate the anisotropic behaviour of captured materials and are a subject of further analysis and modelling. An important observation is the missing reciprocity of an anisotropic highlight that should be in theory replicated in  $\varphi_h$  after  $180^\circ$ .

② **Spatial and spectral averaging** – As our goniometer cannot capture directly BRDFs, we started with the spatial averaging of individual captured SVBRDF images from characteristic slice to obtain a BRDF subdomain  $\theta_h \times \theta_d$  (see Figure 6). Note that for anisotropic slice, we decided to use only a luminance channel of BRDF as independent processing of RGB channels could produce colour artifacts.

③ **Anisotropy weighting in BRDF** – We assume that the BRDF response over  $[\theta_h, \theta_d, \varphi_h]$  is the product of its retro-reflective response (anisotropic slice  $B_A$ ) and its response over  $[\theta_h, \theta_d | \varphi_h]$  (characteristic slice  $B_C$ ). Therefore, all BRDF values along dimensions  $\theta_h, \theta_d, \varphi_h$  (see Figure 6) can be approximated from values of anisotropic  $B_A$  and characteristic  $B_C$  slices by replicating the characteristic slice along  $\varphi_h$  and multiplying it row-wisely by the corresponding column of anisotropic slice as shown in Figure 11.

However, application of the same approach to texture data is not possible, as it artificially increases overall intensity of off-specular dark images and suppress the sparkle texture effect. Figure 12-right shows an example of such an incorrect performance.

④ **Anisotropy shifting in SVBRDF** – The desired sparkle texture is, in case of standard coatings, present in an angular region near specular reflection, i.e. for half-angle elevations  $\theta_h$  close to zero. Therefore, we suggest copying or shifting images corresponding to higher  $\theta_h$  indices to lower ones based on the mean BRDF value of the anisotropic slice.

The principal idea is illustrated in Figure 13, and more detail is provided in the pseudocode below. For each BRDF index  $i_T$  along

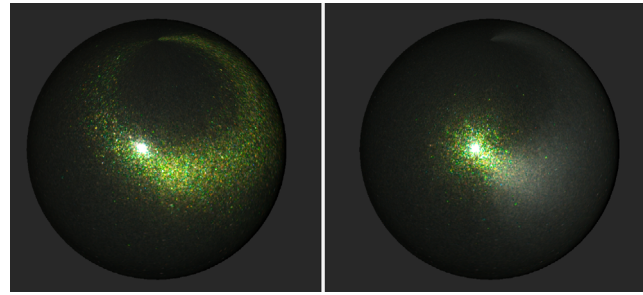
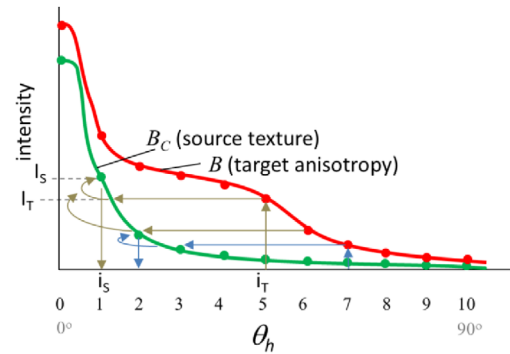


**Figure 12:** A comparison of reference anisotropic measurement (left) and an example of incorrect anisotropic weighting of SVBRDF images (right).



	<i>Input:</i>
1	$B_C$ ... characteristic slice BRDF ( $\theta_h, \theta_d$ )
2	$B$ ... anisotropic BRDF ( $\theta_h, \theta_d, \varphi_h$ )
3	$S_C$ ... characteristic slice SVBRDF ( $\theta_h, \theta_d$ )
4	<b>for</b> all indices along $\varphi_h$
5	<b>for</b> all indices along $\theta_d$
6	<b>for</b> decreasing indices $i_T$ along $\theta_h$ {
7	(a) find index $i_S   i_S < i_T$ along $\theta_h$ where $B_C(i_S, \theta_d) \geq B(i_T, \theta_d, \varphi_h)$
8	(b) compute scaling factor: $s = B(i_T, \theta_d, \varphi_h) / B_C(i_S, \theta_d)$
9	(c) copy and scale corresponding image to anisotropic output: $SVBRDF(i_T, \theta_d, \varphi_h) = s \cdot S_C(i_S, \theta_d)$
	}

**Figure 13:** Algorithm of model anisotropic appearance using  $\theta_h \times \theta_d$  SVBRDF subdomain images shifting for given  $\theta_d$  and  $\varphi_h$ .

$\theta_h$  in the target anisotropic slice, we are looking for index  $i_S$  of  $\theta_h$  in a source characteristic slice having the closest higher intensity  $I_S$  in that slice versus in the anisotropic BRDF  $I_T$  (line 7). Then such  $\theta_h$  index  $i_S$  is used for copying an image from the  $\theta_h \times \theta_d$  source SVBRDF to the output anisotropic SVBRDF (line 9). To achieve smooth transitions between shifted images, we compensate for the difference between target and shifted source intensities by multiplying each image by scaling factor  $s$  (lines 8,9). This process is repeated across all indices of  $\theta_d$  and  $\varphi_h$  to reconstruct complete anisotropic spatially-varying appearance. The proposed approach should in general preserve the total energy of the original BRDF, while reciprocity is controlled by fixing  $\varphi_d$  and by axial symmetry of anisotropic slice as discussed further. The anisotropy shifting

process is very fast, as our MATLAB implementation takes only several seconds.

Note, that in case of anisotropic appearance transfer (explained in Section 7), where we have two materials with significantly different intensities of BRDFs in characteristic and anisotropic slices, an additional user-defined scaling of anisotropic slice intensities might be needed to adjust the intensity of resulting material.

## 7. Anisotropy Parametric Editing and Transfer

Additionally, we propose an optional parametric editing of an anisotropic slice to allow customized anisotropic behaviour and/or its transfer to any isotropic effect coating.

⑤ **Parametric model of anisotropy** – Captured anisotropic slice holds key information about anisotropic behaviour of the material. However, to effectively edit and explore different anisotropic appearances we need to create its simplified parametric model.

Due to a high difference in intensities of specular highlight (in the upper part of the slice, i.e. near  $\theta_h = 0^\circ$ ) and anisotropic highlight of lower intensity near particular azimuth  $\varphi_h$  only, we applied remapping of BRDF intensities proposed in [NJR15]. After remapping, it became clear we need to model independently: (1) the decrease of intensity with increasing  $\theta_h$ , (2) the anisotropic behaviour of specular highlight near  $\theta_h = 0^\circ$  and (3) the azimuthal highlight for  $\theta_h > 5^\circ$ . First, we attempted to fit anisotropic lobes of analytical BRDF models: Ashikhmin–Shirley, Ashikhmin–Premoze, Kurt, Lafortune, Ward [GGG\*16]. Most of the models were not able to correctly represent the anisotropic highlight, possibly due to a limited number of retro-reflective sample points in our anisotropic slice. Moreover, all enlisted models enforced symmetry to the anisotropic slice. Although the symmetry should be correct due to BRDF reciprocity, it was not present in the captured data, which is caused presumably by light refraction and scattering as it travels through a translucent layer of the resin. See our results in supplementary material. To avoid incorrect fitting and at the same time allowing intuitive editing of anisotropy, we resorted to an additive mixture of two Gaussians and an exponential function where the former described specular/anisotropic highlight and the latter intensity decline with increasing  $\theta_h$  as follows

$$f = a_1 \exp\left(-\frac{\theta_h^2}{2\sigma_{\theta_1}^2} - \frac{(\varphi_h - \mu_{\varphi_1})^2}{2\sigma_{\varphi_1}^2}\right) + a_2 \exp\left(-\frac{(\theta_h - \mu_{\theta_2})^2}{2\sigma_{\theta_2}^2} - \frac{(\varphi_h - \mu_{\varphi_2})^2}{2\sigma_{\varphi_2}^2}\right) + c \cdot \exp(w \cdot \theta_h). \quad (1)$$

Each Gaussian is described by a scale  $a$ , its center  $(\mu_\theta, \mu_\varphi)$  and variations  $(\sigma_\theta, \sigma_\varphi)$ . The first Gaussian misses parameter  $\mu_{\theta_1}$  as we assume the specular highlight to be always located at  $\theta_h = 0^\circ$ . The exponential function is described by parameters  $c$  and  $w$ . For the model's parameters fitting was used a standard MATLAB implementation of Levenberg–Marquardt fitting algorithm with default setting of 400 iterations taking about 5 s.

This parametric model is further used for editing of anisotropic behaviour by creating a novel anisotropic slice (Section 8.2). Further, we can use the model to transfer anisotropic properties from

source anisotropic coating to target isotropic coating as it is shown in the Section 8.4.

## 8. Results

### 8.1. Validation of the proposed approach

This section compares the reconstructed SVBRDF data using the proposed anisotropic framework with full captured anisotropic SVBRDF dataset  $n_{\theta_h} \times n_{\theta_d} \times n_{\varphi_h}$  of  $18 \times 5 \times 24 = 2160$  images. Individual texture tiles are stored in an uncompressed binary format and are directly accessed using lookup functions in our OpenGL rendering application. A linear interpolation is used for the obtaining of non-measured directions. We used a linear interpolation from the two closest directions along each of three dimensions. For coatings rendering we used a sphere and a car-like shape common for coating demonstration purposes in the coating industry. See the supplementary material. Figure 14-(a) shows renderings of full captured reference appearance data for a point-light illumination. To enforce isotropic appearance, we can use just a characteristic slice  $\theta_h \times \theta_d$  (see Figure 6) of captured images selected for fixed  $\varphi_h$ . To get similar near specular behaviour to original anisotropic data, we select  $\varphi_h$  corresponding to the  $\theta_h \times \theta_d$  subspace having the closest similarity to the mean subspace across all azimuths. Such rendered  $\theta_h \times \theta_d$  subdomain with enforced isotropic appearance, i.e. using the same  $\theta_h \times \theta_d$  subspace regardless the azimuthal angle  $\varphi_h$ , is shown in Figure 14(b). Results of the proposed framework reconstructing this data using captured anisotropic and characteristic data slices are shown in Figure 14(c). Finally, Figure 14(d) shows results obtained by additional modelling of the captured anisotropic slice using the parametric model proposed in Section 7. All renderings comprise an inset image showing a difference from the reference scaled  $3\times$ . We have found, that capturing of only anisotropic and characteristic slices instead of a full dataset  $\theta_h \times \theta_d \times \varphi_h$  without anisotropic slice modelling introduced negligible visual errors for all of the tested materials.

### 8.2. Anisotropic behaviour editing

One can edit also anisotropy of the measured material by parameters modification of the proposed anisotropic model fitted to grey scale reflectance data of the anisotropic slice.

We fitted model parameters for all four coatings. The optimized parameters and their fitting bounds are shown in the supplementary material.

Original data of anisotropic slice and their fitting for two tested samples are shown in Figure 15. The fittings of the near specular anisotropy are not always perfect (e.g. specular highlight of *coating4*) due to a limitation of using two Gaussian lobes only. Note that modelling of anisotropic slice can introduce errors impacting energy conservation. We propose relatively simple model with few parameters only to facilitate intuitive editing of anisotropic behaviour. Our approach still yields satisfactory rendering behaviour as shown in Figure 14(d). The last row of images shows results of our approach combining parametric modelling of the anisotropic slice in combination with  $\theta_h \times \theta_d$  SVBRDF subdomain measurements using the proposed image shifting along  $\theta_h$ . The inset difference

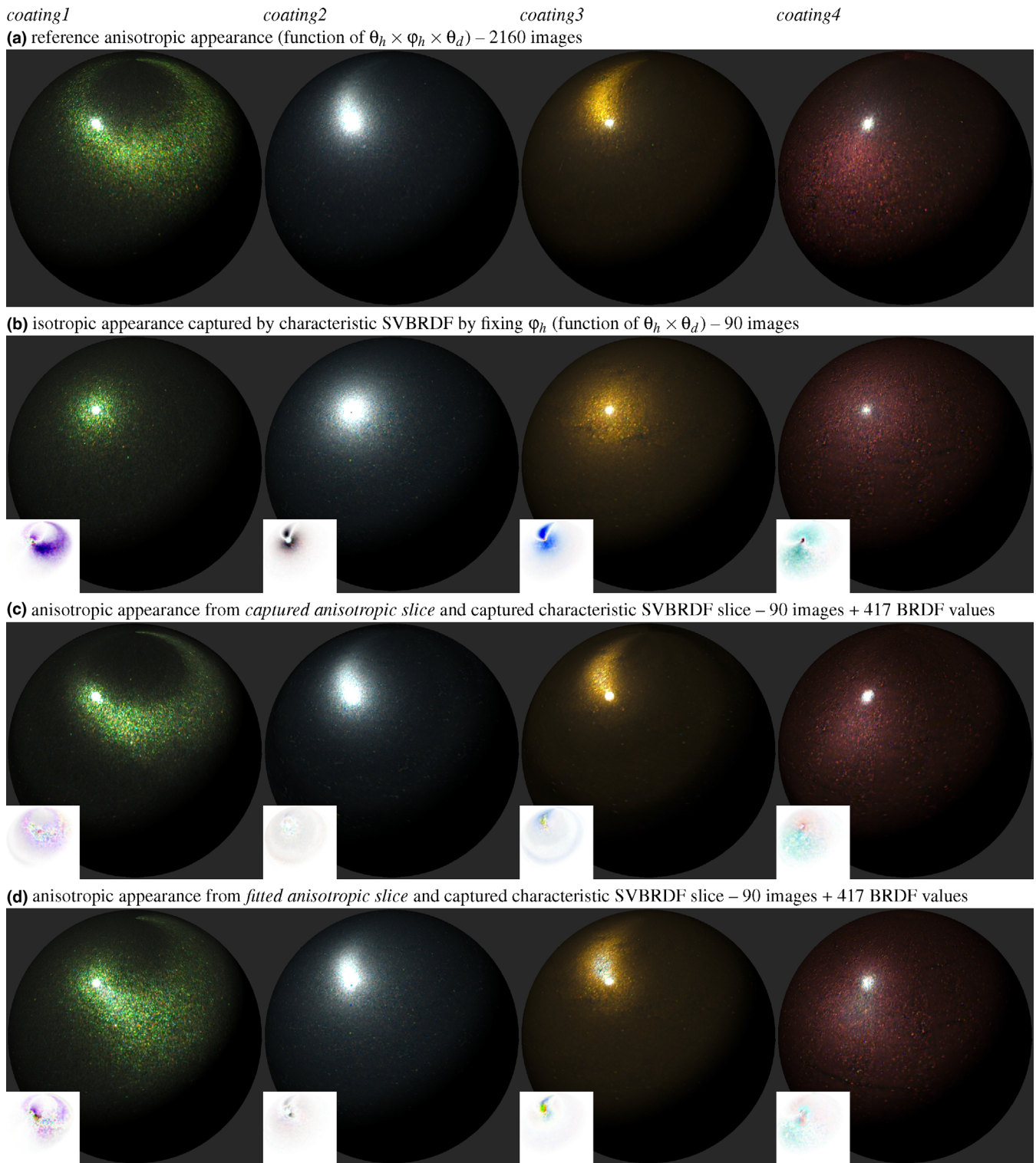


**Figure 14:** Anisotropic appearance properties of effect coatings: (a) captured samples using reference anisotropic SVBRDF, (b) its subset of isotropic  $(\theta_h \times \theta_d)$  appearance subdomain, (c) anisotropy reconstruction using measured anisotropic BRDF slice and characteristic SVBRDF slice, (d) the same as (c) but including the parametric modelling of the anisotropic slice. Inset images show a difference from the reference scaled  $3\times$ .

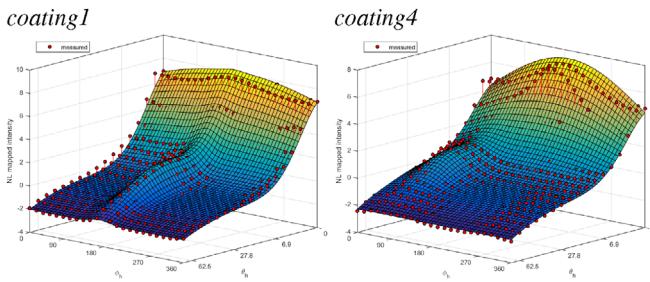


**Figure 15:** Examples of fitting a parametric model to anisotropic behaviour represented by anisotropic slice (red dots represent the measured data points).

images show increase of error especially close to specular highlight, but the original anisotropic behaviour is still reliably conveyed. A detailed comparison in movies for different alignment of anisotropy axis and moving point-light is given in a supplementary material. Our model performance in Figure 15 suggests that it could be improved by using a more heavy-tailed distribution such as Cauchy, Lévy, or t-distribution. To achieve even better results at the cost of more parameters, one can use other surface modelling methods, e.g. splines.

The proposed parametric model allows an intuitive editing of an anisotropic slice that is responsible for final anisotropic behaviour. An example of such editing is given in Figure 16, where we compare original appearance of *coating1* with its variation obtained by scaling intensity and/or width of anisotropic highlight. Although different manipulations are possible, one can hit the angular sampling limit of the source  $\theta_h \times \theta_d$  SVBRDF data, resulting, e.g. in sharp boundaries of anisotropic highlights as shown in the right image of Figure 16.

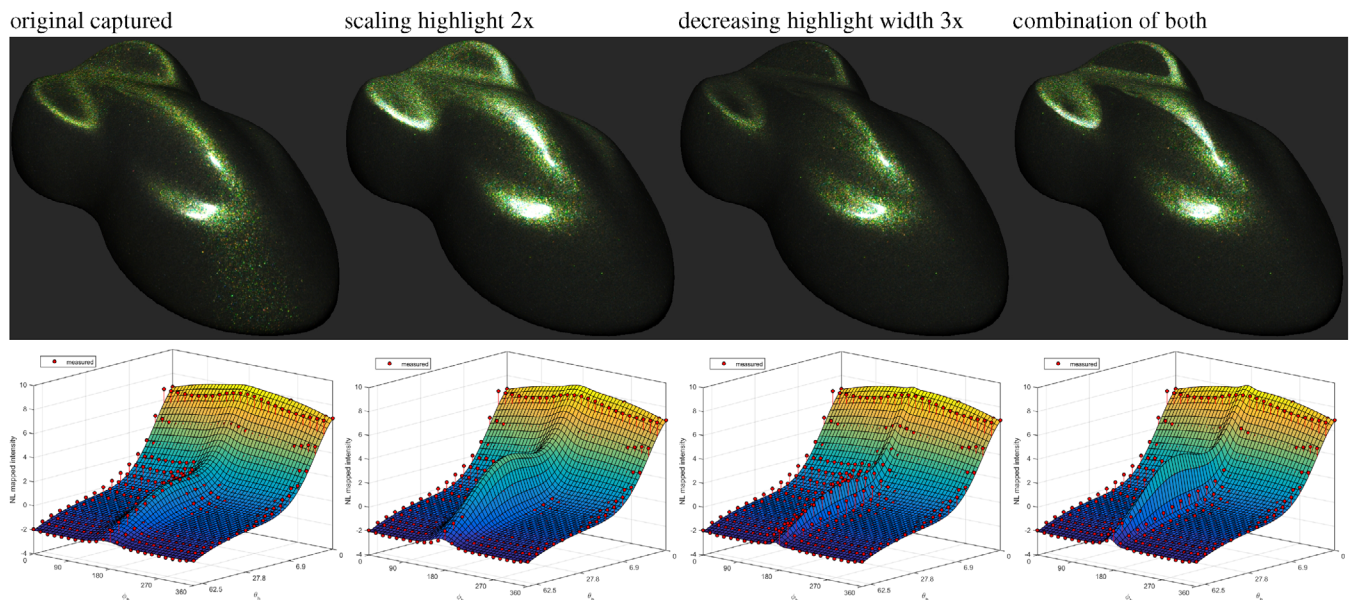


**Figure 16:** Editing of model parameters to create customized anisotropic behaviour.

### 8.3. A psychophysical validation

We also ran an online psychophysical validation study with 55 subjects to assess visual fidelity of the proposed framework. Subjects were shown stimuli images with three side-by-side renderings: the isotropic characteristic SVBRDF slice (Figure 14b), the original anisotropic SVBRDF data (Figure 14a), and the result of our parametric anisotropic model combined with the isotropic slice (Figure 14d). They were asked to assess the difference between the original and our model on a scale 0–10, given the distance between isotropic and original data is 10. Out of the subjects' responses, we computed a mean opinion score and obtained the following values for all four tested materials: *coating1* - 3.9, *coating2* - 3.8, *coating3* - 4.5, *coating4* - 4.9. Results show that on average the joint error introduced by the proposed data reconstruction from the characteristic SVBRDF slice, and by parametric modelling of the anisotropic slice, represents 40% of the total perceived anisotropic behaviour. We consider this result as acceptable, as subjects could also consider differences on a local flake level; however they are not important as our method does not preserve per-pixel behaviour. We should also note that the parametric model which is the main source of visual differences is needed only for anisotropy editing. Once we use original captured anisotropic slice, we obtain much better results (see Figure 14c).

### 8.4. Transfer of anisotropic behaviour

The main advantage of the proposed model, is its capability to introduce anisotropic behaviour to isotropic effect coatings. This demonstrates how their appearance would change when achieving uniform alignment of its pigment flakes. This so called *anisotropy transfer* is approximated by supplying the  $\theta_h \times \theta_d$  SVBRDF isotropic measurements and applying to them anisotropic behaviour (represented by the anisotropic slice) to them, either recorded from a different

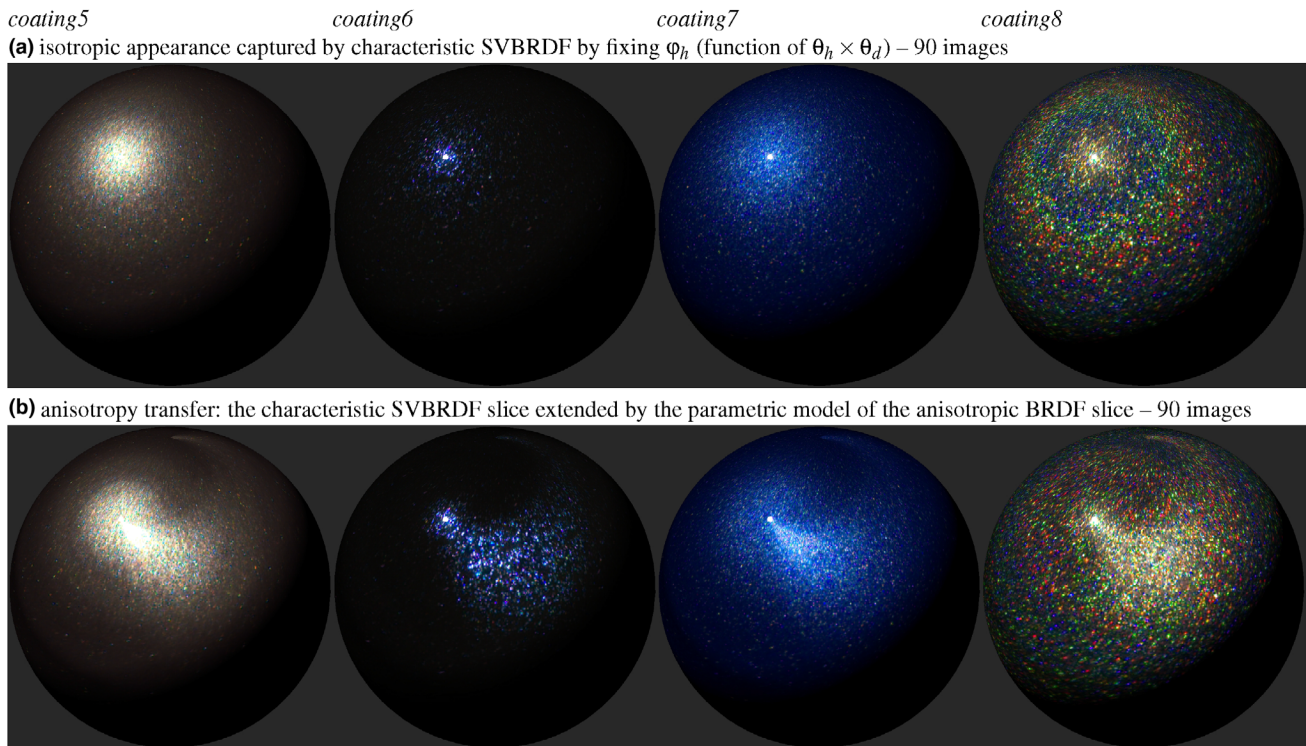


**Figure 17:** Result of anisotropic behaviour transfer from coating1 (see Figure 14) to four coatings captured as isotropic using  $\theta_h \times \theta_d$  representation: (a) original isotropic, (b) anisotropic appearance transfer.

material, or manually tuned by a user, as was shown in Section 8.2. Figure 17 shows example of anisotropy transfer from *coating1* to four isotropic coatings captured as characteristic SVBRDF slice. In all cases, we observe a more visually rich behaviour introduced by the anisotropic highlight.

### 8.5. Exploring anisotropic behaviour

A location of anisotropic highlight depends on the direction of particles' alignment over the surface. This can be simulated simply by a change of UV mapping of coating texture while respecting a change of local illumination and viewing angles as is shown in Figure 18. In the case of magnetic pigment application, this can be achieved either by a direction of pigment contact application or by using a directional electromagnetic field.

We consider the proposed framework as convenient tool for colour designers to explore appearance of their coatings under different anisotropic patterns and their azimuthal alignment. See supplementary video of different anisotropy axis alignments. Note that in the video the positions of object, light, and camera are fixed and only azimuthal alignment of pigment particles is changing, demonstrating flakes' alignment-dependent effects.

## 9. Discussion and Method's Limitations

The proposed approach benefits from a low number of captured images representative of illumination and viewing direction-dependent

effect coatings behaviour. However, we represent anisotropic behaviour at particular angles, by images captured for different angles  $\theta_h$ . Thus, it may happen that for the reproduction of grazing angles are used images captured at low elevation angles. Although this shift along  $\theta_h$  is not physically correct, it does not suppress the sparkle texture effect. This is one of the most important features of effect coatings. Our approach is still based on captured image data, without the need to rely on any statistical flake-based modelling approaches. Due to this fact, the proposed method is universal and not dependent on any specific assumptions or a type of effect coating. It works well for metallic and interference effect pigments and their combinations. We obtained also promising results for goniochromatic coatings using interference effect pigments, i.e. those changing colour with elevation angle of incoming light (along  $\theta_d$ ) as shown in Figure 17–*coating6*. The only coating type requiring extra attention when using our method is the one containing a diffractive pigment shown in Figure 17–*coating8*. Although the anisotropic shifting method works well in this case, for some specific anisotropic functions it might happen that the shifting algorithm would start to move the rainbow area of the first order diffractive highlight to different angular locations, possibly resulting in a physically implausible appearance.

The proposed anisotropy measurement process and coating representation using characteristic and anisotropic slices preserves original physical properties of material, namely reciprocity and energy conservation. Our measurement process captures only BRDF sub-domain, i.e. omits dependency on  $\varphi_d$ . Although its impact on total

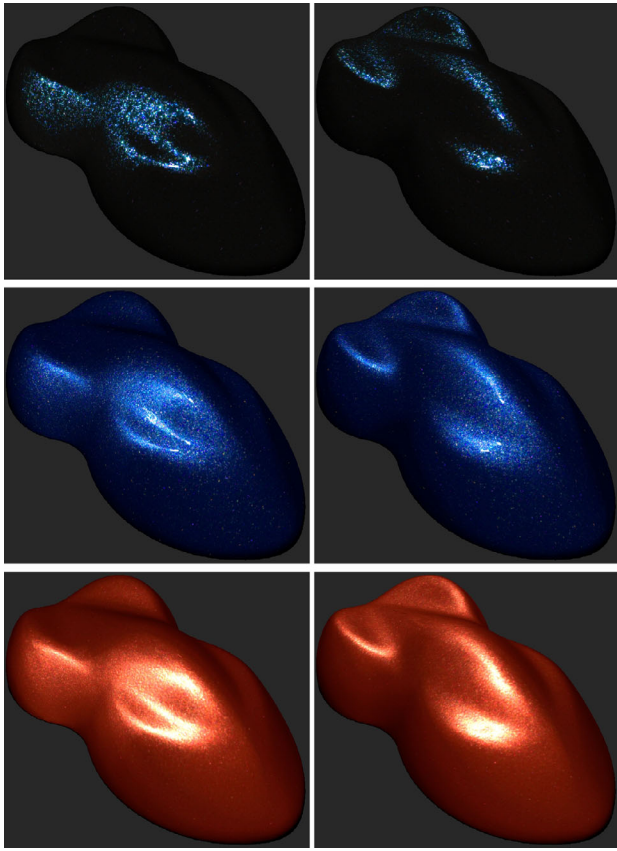


**Figure 18:** Anisotropic appearance transferred from coating1 to three different coatings with isotropic azimuthal distribution of particles (rows). Columns show two azimuthal alignments of pigment particles  $90^\circ$  apart.

energy should be very low [FV19], we cannot guarantee exact energy conservation.

Much more important for energy conservation is a parametric model of anisotropy. We have proposed the model balancing quality and editing abilities, but one can use a much more accurate modelling of anisotropic slice to avoid these sources of error. Our captured representation should recover reciprocity as (a) neglecting  $\varphi_d$  [RVZ08] and (b) representation of individual  $\theta_h \times \theta_d$  subdomains at different  $\varphi_h$  by only a single one, have minimal effect on reciprocity.

Again most important relative to this is accurate modelling of the anisotropic slice. Unfortunately, the captured anisotropic slices of our samples have shown that reciprocity does not hold (see Figure 10), which might be a reason why its modelling using standard BRDF models [GGG\*16] did not work well. On the other hand, one could apply these models in modelling anisotropic slices of truly reciprocal materials. Further, when applying the model to anisotropy transfer or editing, we obtain novel materials with modified anisotropic highlights and thus especially energy conservation cannot hold.

Finally, the capturing of spatially-varying appearance in the proposed slices not only greatly reduces a total number of captured im-

ages and consequently a measurement time, but also allows a convenient acquisition without need for complicated devices. All data can be recorded, e.g. by using a half-circular arc outfitted with several lights and cameras having an axis of rotation parallel with the sample surface. While for capturing of the characteristic slice one needs to rotate the arc over the sample, for capturing the anisotropic slice one needs to fix the arc on the top and rotate the material.

## 10. Conclusions

This paper proposes a novel method of capturing and editing anisotropic behaviour of effect coatings. As a source of anisotropic behaviour, we created a test set of four samples. We proposed an efficient image-based data acquisition based in angular slices on half-difference parameterization. Our parametric model can reproduce anisotropic behaviour and can be used as a template for enhancing appearance of isotropic materials. Thus, the proposed framework allows editing of anisotropic appearance and its transfer to almost any effect coating. This method allows users to rapidly explore and assess the visual benefit of anisotropy in effect coatings in virtual environments. They can create desired appearance by utilizing a combination of anisotropic highlight modelling and its appropriate azimuthal alignment over the coated object body. The captured data are made publicly available for research purposes at <http://btf.utia.cas.cz>.

## Acknowledgements

This research has been supported by the Czech Science Foundation grant 17-18407S.

## References

- [Bel18] BELCOUR L.: Efficient rendering of layered materials using an atomic decomposition with statistical operators. *ACM Transactions on Graphics (TOG)* 37, 4 (2018), 1–14.
- [Bur] B. Burley, BRDF related resources. <http://wiki.nuaj.net/index.php?title=BRDF>. Accessed: 20 July 2020.
- [CDP\*14] CHEN G., DONG Y., PEERS P., ZHANG J., TONG X.: Reflectance scanning: estimating shading frame and BRDF with generalized linear light sources. *ACM Transactions on Graphics (TOG)* 33, 4 (2014), 1–11.
- [DHd16] DUPUY J., HEITZ E., D'EON E.: Additional progress towards the unification of microfacet and microflake theories. In *Eurographics Symposium on Rendering - Experimental Ideas & Implementations*, Eurographics Association, Goslar, Germany (2016).
- [DJ18] DUPUY J., JAKOB W.: An adaptive parameterization for efficient material acquisition and rendering. *ACM Transactions on Graphics (TOG)* 37, 6 (2018), 1–14.
- [DvGNK99] DANA K., VAN GINNEKEN B., NAYAR S., KOENDERINK J.: Reflectance and texture of real-world surfaces. *ACM Transactions on Graphics* 18, 1 (1999), 1–34.

- [DWT\*10] DONG Y., WANG J., TONG X., SNYDER J., LAN Y., BEN-EZRA M., GUO B.: Manifold bootstrapping for SVBRDF capture. *ACM Transactions on Graphics* 29, 4 (July 2010), 98:1–98:10.
- [Fil15] FILIP J.: Analyzing and predicting anisotropic effects of BRDFs. In *ACM Symposium on Applied Perception* (2015), pp. 25–32.
- [FK18] FILIP J., KOLAFOVÁ M.: Effects of surface anisotropy on perception of car body attractiveness. In *Proceedings of the 26th Pacific Conference on Computer Graphics and Applications: Short Papers* (2018), PG '18, pp. 17–20.
- [FV15] FILIP J., VAVRA R.: Anisotropic materials appearance analysis using ellipsoidal mirror. In *IS&T/SPIE Conference on Measuring, Modeling, and Reproducing Material Appearance, paper 9398-25* (2015).
- [FV19] FILIP J., VÁVRA R.: Image-based Appearance Acquisition of Effect Coatings. *Computational Visual Media*, 5 (2019), 73–89.
- [FVH\*13] FILIP J., VAVRA R., HAINDL M., ZID P., KRUPICKA M., HAVRAN V.: BRDF slices: Accurate adaptive anisotropic appearance acquisition. In *Conference on Computer Vision and Pattern Recognition, CVPR* (2013), pp. 4321–4326.
- [GGG\*16] GUARNERA D., GUARNERA G. C., GHOSH A., DENK C., GLENCROSS M.: BRDF representation and acquisition. *Computer Graphics Forum* 35, 2 (2016), 625–650.
- [HHE08] HANSEN B. C., HAUN A. M., ESSOCK E. A.: The horizontal effect: A perceptual anisotropy in visual processing of naturalistic broadband stimuli. In *Visual Cortex: New Research*. Nova Science Publishers, Inc., January 2008.
- [JdJM14] JAKOB W., D'EON E., JAKOB O., MARSCHNER S.: A comprehensive framework for rendering layered materials. *ACM Transactions on Graphics (ToG)* 33, 4 (2014), 1–14.
- [KHx\*19] KUZNETSOV A., HASAN M., XU Z., YAN L.-Q., WALTER B., KALANTARI N. K., MARSCHNER S., RAMAMOORTHY R.: Learning generative models for rendering specular microgeometry. *ACM Transactions on Graphics* 38, 6 (2019), 225–1.
- [Koe84] KOENDERINK J. J.: The structure of images. *Biological Cybernetics* 50, 5 (1984), 363–370.
- [LDPT13] LAN Y., DONG Y., PELLACINI F., TONG X.: Bi-scale appearance fabrication. *ACM Transactions on Graphics* 32, 4 (July 2013), 145:1–145:12.
- [LKH12] LANS I. v. d., KIRCHNER E., HALF A.: Accurate appearance-based visualization of car paints. In *Conference on Colour in Graphics, Imaging, and Vision* (2012), Society for Imaging Science and Technology, pp. 17–23.
- [LKK00] LU R., KOENDERINK J. J., KAPPERS A. M.: Specularities on surfaces with tangential hairs or grooves. *Computer Vision and Image Understanding* 78, 3 (2000), 320–335.
- [MHH\*12] MCAULEY S., HILL S., HOFFMAN N., GOTANDA Y., SMITS B., BURLEY B., MARTINEZ A.: Practical physically-based shading in film and game production: Physically-based shading at disney. In *ACM SIGGRAPH 2012 Courses* (2012), SIGGRAPH '12, pp. 10:1–10:7.
- [MPR05] MAILE F. J., PFAFF G., REYNERS P.: Effect pigments: past, present and future. *Progress in Organic Coatings* 54, 3 (2005), 150–163.
- [MSS\*12] MALZBENDER T., SAMADANI R., SCHER S., CRUME A., DUNN D., DAVIS J.: Printing reflectance functions. *ACM Transactions on Graphics* 31, 3 (June 2012), 20:1–20:11.
- [NJR15] NIELSEN J. B., JENSEN H. W., RAMAMOORTHY R.: On optimal, minimal BRDF sampling for reflectance acquisition. *ACM Transactions on Graphics* 34, 6 (2015), 186:1–186:11.
- [NRH\*77] NICODEMUS F., RICHMOND J., HSIA J., GINSBURG I., LIMPERIS T.: Geometrical considerations and nomenclature for reflectance. *NBS Monograph 160* (1977), 1–52.
- [OVW11] ONS B., VERSTRAELEN L., WAGEMANS J.: A computational model of visual anisotropy. *PLoS ONE* 6, 6 (2011), e21091.
- [Pfa08] PFAFF G.: *Special Effect Pigments: Technical Basics and Applications*. Vincentz Network GmbH & Co KG, Hannover, 2008.
- [PLMR17] PEREIRA T., LEME C. L. A. P., MARSCHNER S., RUSINKIEWICZ S.: Printing anisotropic appearance with magnetic flakes. *ACM Transactions on Graphics* 36, 4 (July 2017), 123:1–123:10.
- [RGB\*14] RAYMOND B., GUENNEBAUD G., BARLA P., PACANOWSKI R., GRANIER X.: Optimizing BRDF orientations for the manipulation of anisotropic highlights. *Computer Graphics Forum* 33, 2 (2014), 313–321.
- [RSK09] RUMP M., SARLETTE R., KLEIN R.: Efficient resampling, compression and rendering of metallic and pearlescent paint. In *Vision, Modeling, and Visualization* (2009), pp. 11–18.
- [Rus98] RUSINKIEWICZ S.: A new change of variables for efficient BRDF representation. In *Rendering Techniques '98* (1998), pp. 11–22.
- [RVZ08] ROMEIRO F., VASILYEV Y., ZICKLER T.: Passive reflectometry. In *Proceedings of the 10th European Conference on Computer Vision: Part IV* (2008), ECCV '08, pp. 859–872.
- [SM10] SHIMIZU C., MEYER G. W.: Color styling tools. In *Color and Imaging Conference* (2010), Society for Imaging Science and Technology, pp. 272–279.
- [SM15] SHIMIZU C., MEYER G. W.: A computer aided color appearance design system for metallic car paint. In *Color and Imaging Conference* (2015), Society for Imaging Science and Technology, pp. 93–102.

- [SPGC08] SHAH P., PADILLA S., GREEN P., CHANTLER M.: Perceived directionality of  $1/f^\beta$  noise surfaces. In *ACM Symposium on Applied Perception in Graphics and Visualization, 2008* (2008), p. 203.
- [VWH18] VELINOV Z., WERNER S., HULLIN M. B.: Real-time rendering of wave-optical effects on scratched surfaces. *Computer Graphics Forum* 37, 2 (2018), 123–134.
- [WH04] WENK H.-R., HOUTTE P. V.: Texture and anisotropy. *Reports on Progress in Physics* 67, 8 (2004), 1367.
- [WPMR09] WEYRICH T., PEERS P., MATUSIK W., RUSINKIEWICZ S.: Fabricating microgeometry for custom surface reflectance. *ACM Transactions on Graphics* 28, 3 (July 2009), 32:1–32:6.
- [WVJH17] WERNER S., VELINOV Z., JAKOB W., HULLIN M. B.: Scratch iridescence: Wave-optical rendering of diffractive surface structure. *ACM Transactions on Graphics* 36, 6 (Nov. 2017), 207:1–207:14.
- [XSD\*13] XU K., SUN W.-L., DONG Z., ZHAO D.-Y., WU R.-D., HU S.-M.: Anisotropic spherical Gaussians. *ACM Transactions on Graphics* 32, 6 (Nov. 2013), 209:1–209:11.
- [YHJ\*14] YAN L.-Q., HAŠAN M., JAKOB W., LAWRENCE J., MARSCHNER S., RAMAMOORTHY R.: Rendering glints on high-resolution normal-mapped specular surfaces. *ACM Transactions on Graphics* 33, 4 (July 2014), 116:1–116:9.
- [YHMR16] YAN L.-Q., HAŠAN M., MARSCHNER S., RAMAMOORTHY R.: Position-normal distributions for efficient rendering of specular microstructure. *ACM Transactions on Graphics (TOG)* 35, 4 (2016), 1–9.
- [YHW\*18] YAN L.-Q., HAŠAN M., WALTER B., MARSCHNER S., RAMAMOORTHY R.: Rendering specular microgeometry with wave optics. *ACM Transactions on Graphics (TOG)* 37, 4 (2018), 1–10.
- [ZJ18] ZELTNER T., JAKOB W.: The layer laboratory: a calculus for additive and subtractive composition of anisotropic surface reflectance. *ACM Transactions on Graphics (TOG)* 37, 4 (2018), 1–14.

### Supporting Information

Additional supporting information may be found online in the Supporting Information section at the end of the article.

**Table 1:** Fitted parameters for modelling of anisotropic slice for all measured materials.

**Table 2:** Fitting bounds of model's parameters.

**Figure 1:** Fitting a parametric model to anisotropic behaviour represented by anisotropic slice (dots represent the measured data points).

**Data Video S1**

**Data Video S2**

**Data Video S3**

**Data Video S4**

**Data Video S5**